Markov Radom Field Modeling for Fusion and Classification of Multisource Remotely Sensed Images

Radja Kheddam
Image Processing and Radiation Laboratory
Faculty of Electronic and Computer Science
USTHB, Algiers, Algeria

Aichouche Belhadj-Aissa
Image Processing and Radiation Laboratory
Faculty of Electronic and Computer Science
USTHB, Algiers, Algeria

ABSTRACT
In this paper, we discuss a Markov Random Field (MR) modeling for multisource and multitemporal remotely sensed image fusion and classification. Satellite images provided by individual sensor are incomplete, inconsistent or imprecise. Additional sources may provide complementary information and the fusion of multisource data can create a more consistent interpretation of the scene in which the associated uncertainty is decreased and the reliability of analysis results is increased. Also, a temporal data from a single sensor can be considered as separate information sources. The combination of multitemporal data over the same scene enhances information on changes that might have occurred in the area observed over time. Using these available data through a fusion and classification process, our objective is to extract more information to achieve greater accuracy in assigning pixels to thematic classes. The best methodological framework which allows the realization of this process is a Markov Random Field (MRF).

Keywords
Markov Random Field (MRF), Satellite Images, Fusion, Classification.

1. INTRODUCTION
Extraction of land-cover information is usually achieved through a classification process which is one of the most powerful tools in digital image processing. Its objective is to use the data contained in remotely sensed images (multispectral, multisource, or multitemporal) we are analyzing to extract information and identify targets into a defined number of *thematic classes*. Multispectral, multisource and multitemporal classification techniques are relevant to contextual data fusion domain [3], [15]. Based upon the works of Schistad Solberg [12], [13], three kinds of context have been defined: 1) spectral context, 2) spatial context and 3) temporal context. The spectral context refers to different bands of the electromagnetic spectrum of the same sensor or of two or more different sensors. Using multispectral or multisource image frequently improves the separation between various ground cover classes compared to a single band image analysis. The spatial context is defined by the correlation between spatially adjacent pixels in a spatial neighborhood. The temporal context is considered between multiple images of the same area taken at different instants. Temporal contextual information deals with the consideration of the change of class identity over time. Accordingly, contextual information is important for the interpretation of a scene [10]. When a pixel is considered in isolation, it may provide incomplete information about the desired characteristics. However, the consideration of the pixel in its context, more complete information might be derived. By merging multisource and multitemporal data with spatial information, the classification accuracy is improved. The best methodological framework which allows the realization of this contextual fusion process is a Markov Random Field (MRF) [7], [10] [13]. MRF is able to model and capture the three kinds of context. This paper is organized as follows. In section 2, we present basic elements of MRF contextual single source classification, while sections 3 and 4 describe respectively MRF multisource classifier and MRF multitemporal classifier. Developed Markovian process is applied on two satellite images (HRV/SPOT and ETM+/Landsat) covering both the north-eastern part o Algiers (Algeria). Experimental results are presented and discussed in section 5. Finally, section 6 concludes this paper.

2. MRF SINGLE SOURCE CLASSIFICATION
We assume that a classified image X and observed data Y are realizations of stochastic processes X and Y, respectively. Multispectral data $Y_p = \{ Y^1, Y^2, ..., Y^k \}$ which are observed through K spectral bands of specified sensor p, are supposed to be acquired on a finite lattice $W = \{s = (i, j) : 1 <= s <= S \}$, s is the site of the ijth pixel and S lattice's area.. The set $Y_k = \{y_s^k, ..., y_S^k\}$ where k = 1, 2, …K, denotes the data taken at the kth wavelength, where $y_s^k \in \{ 1, 2,...NG-1 \}$ and NG is the number of observable gray levels. It is also possible to describe the multispectral data with $Y = \{ y_s, 1 <= s <= S \}$ where $y_s = \{ y_s^1, y_s^2, ..., y_s^k \}$ is a feature vector observed on the site s called also a spectral signature on site s. Our goal is to find the optimal classified image $X^* = \{ xs, ..., xS \}$ based on the observed data Y. Each site of the segmented image is to assigned into one of M classes; that is, $x^*_s = \{ 1, 2, ..., M \}$ where M is the number of classes and assumed to be known in supervised classification process. This optimization is executed from the view point of the maximum a posterior (MAP) estimation [2] as follows:

$$X^* = X_{MAP} = \underset{X}{argmax}\{P(X/Y)\} \quad (1)$$

Following Bayes theorem, equation (1) becomes:

$$X^* = X_{MAP} = \underset{X}{argmax}\left\{\frac{P(Y/X)P(X)}{P(Y)}\right\} \quad (2)$$

Modeling of both class conditional distribution *P(Y/X)* and prior distribution *P(X)* becomes an essential task. *P(Y)* is the probability distribution of the observed data and doesn't depend on the labeling *X*. Note that the estimate (2) becomes the pixel–wise non–contextual classifier if the prior probability doesn't have any consequence in formulating (2). *P(Y/X)* is the conditional probability distribution of the observation *Y* given the labeling *X*. It's usually assumed that this probability at each site is independent of its neighbors:

$$P(Y/X) = \prod_S^S P(y_s/X) = \prod_S^S P(y_s/x_s) \quad (3)$$

A commonly used model for *P(Y/X)* is that the feature vector observed Y_s is drawn from a Gaussian distribution which gives:

$$P(y_s/x_m) = \frac{1}{\sqrt{(2\pi)^k \left|\sum_{x_m}\right|}} exp\left\{-\frac{1}{2}\left(y_s - \mu_{x_m}\right)^T . \sum_{x_m}^{-1} . \left(y_s - \mu_{x_m}\right)\right\} \quad (4)$$

Where μ_{xm} and Σ_{xm} are respectively the mean vector and the covariance matrix of each class x_m with $m = 1, 2, \ldots M$. For a Markov random field X, the conditional distribution of a point in the field given the all other points is only dependent on its neighbors:

$$P(x_s / x_{S-s}) = P(x_s / x_{NS}) \quad (5)$$

Where *S-s* denotes a set of points in S excluding s and Ns is neighboring points of pixel s. The first order of neighborhood system is usually defined as the four pixels surrounding a given pixel, and higher orders are defined by adding corner pixels to a lower order neighborhood system. According to the Hammerslay-Clifford theory, $P(x_s / x_{Ns})$ can be expressed as a Gibbs distribution:

$$P(x_s / x_{Ns}) = \frac{1}{Z} exp\left\{\sum_{q \in Q}\left(-V^q(x_s / x_{Ns})\right)\right\} \quad (6)$$

Where Z is a normalizing constant, Q is the set of all cliques q in the neighborhood of the site s and $V^q(x_s / x_{Ns})$ is the potential function whose value depends on clique q and x_s. Our objective is to estimate the class label of a pixel on site s given the estimates of class labels for all other pixels inside the lattice *S*. Then, the optimization problem of equation (1) becomes:

$$x_s^* = \underset{x_s}{argmax}\left\{P(x_s / Y, x_{S-s}^*)\right\} \quad (7)$$

Applying the Bayes rule and considering the Markov property of equation (5), the argument of (7) becomes:

$$P(x_s / Y, x_{S-s}^*) = P(Y / x_s, x_{S-s}^*) . P(x_s / x_{S-s}^*) \quad (8)$$

By virtue of equation (3), the first term of the right hand of (8) becomes:

$$P(Y / x_s, x_{S-s}^*) = P(y_s / x_s) . P(y_{S-s} / x_{S-s}^*) \quad (9)$$

Since the class assignment of all other pixels excepted xs inside the lattice are already made, the probability $P(y_{S-s} / x^*_{S-s})$ is not a factor affecting the optimization. Therefore, (7) in connection with (8) and (9) becomes:

$$x_s^* = \arg\max\left\{P(y_s / x_s) . P(x_s / x_{Ns}^*)\right\} \quad (10)$$

Let be $U(y_s/x_s) = -logP(y_s/x_s)$ the negative of the log-likelihood of the class conditional distribution and $U(x_s/x^*_{Ns}) = -logP(x_s/x_{Ns}) = -logP(x_s/x^*_{Ns})$ the positive energy function which corresponds to the transition probability inside a clique including point s. Applying the negative logarithm both to equation (4) and (6), substituting into (10), the MAP estimate of the true class label as given by equation (1) is equivalent to the minimization of the a posterior energy function:

$$x_s^* = \arg\min\left\{U(y_s/x_s) + U(x_s / x_{Ns})\right\} \quad (11)$$

That is:

$$x_s^* = \underset{x_s}{argmin}\left\{\frac{1}{\sqrt{(2\pi)^k \left|\sum_{x_m}\right|}} exp\left\{-\frac{1}{2}\left(y_s - \mu_{x_m}\right)^T . \sum_{x_m}^{-1} . \left(y_s - \mu_{x_m}\right)\right\} + \sum_{q \in Q}\left(V^q(x_s/x_{Ns})\right)\right\} \quad (12)$$

The first term on the right hand of (12) is considered as energies of cliques of order 1 and is often used to provide an initial configuration for the contextual classification process. The second term through which the spatial context is introduced, defines energies of cliques of higher order and corresponds to the transition probability inside a clique including point s. Ising and Potts models are frequently used as energy function model for image segmentation problem. In the last few years, some more complex models have been proposed. One of these models using recent developments in statistics is "chien model" [5]. In our case we have chosen the followed Potts model variant [7]:

$$V^q(x_s) = \beta_{spa} . I(x_s, x_{r \in Ns}) \quad (13)$$

The parameter β_{spa}, a user specified is a weight emphasizing the significance of interactions among adjacent pixels inside the clique. *I (,)* is a potential function given by:

$$I(x_s, x_{r \in Ns}) = \begin{cases} 1 & if \quad r \neq s \\ 0 & if \quad r = s \end{cases} \quad (14)$$

This model corresponds to counting the total number of neighboring points of different value in s in a clique q. Substituting equation (13) into equation (12), the energy function to minimize becomes:

$$x_s^* = \underset{x_s}{argmin}\left\{\frac{1}{\sqrt{(2\pi)^k \left|\sum_{x_m}\right|}} exp\left\{-\frac{1}{2}\left(y_s - \mu_{x_m}\right)^T . \sum_{x_m}^{-1} . \left(y_s - \mu_{x_m}\right)\right\} + \beta_{spa} \sum_{r \in q \in Q} I(x_s, x_r)\right\} \quad (15)$$

To solve equation (15), much literature exists on optimization algorithms [9]. Simulated Annealing (SA) [6] can be used to find an iterative solution, but its computational demands are well known. A computationally feasible alternative to the SA algorithm is Besag's Iterated Conditional Modes (ICM) algorithm [1] which converges to a local minimum of the energy function. Only the ICM algorithm was used in tests reported here and is presented in four steps [7], [8]:

Step1: Estimate statistic parameters set (μ_{xm}, Σ_{xm}) from the training samples of each class m of the observed data;

Step2: Estimate an initial classification using the non-contextual pixel-wise maximum likelihood decision rule (equation 4);

Step3: Perform the local minimization defined by equation (15) at each pixel in specified order: update x^*_s by the class x_s that minimizes equation (15);

Step4: Repeat step (2) until convergence. Iterative algorithms often pose convergence problem. Convergence criterion which we have adopted in this study is a zero number of pixels changing classes between two consecutive iterations. This number of pixels is calculated on the whole image and thus for all classes. We have thought of a local criterion convergence which can be regarded as a zero number of pixels which change state on each class, other classes being masked. This procedure can be seen as the decomposition of ICM process on a number of under-processes. Each under-process relates to one class and is slow or fast according to the heterogeneity of this class.

3. MRF MULTISOURCE CLASSIFICATION

Multisource classification performs fusion on a pixel level by merging the posterior probabilities from sensor-specific

classifier, taking into account the reliability factor of each sensor. This factor can be defined as the overall accuracy for each single source classifier. Let the set $(Y_1, Y_2, \ldots, Y_n)$ be the observed data acquired respectively by sensors *1, 2, …n,* and $P(Y_1, Y_2, \ldots, Y_n/X)$ the conditional probability density of the set $(Y_1, Y_2, \ldots, Y_n)$ given the scene labels *X*. The task is to assign each pixel to the class that maximizes the posterior probability $P(X/Y_1, Y_2, \ldots, Y_n)$. In a Bayesian formulation, the relationship between the measurements and the prior information is given by [7], [12], [13]:

$$P\left(X/Y_1,Y_2,\ldots,Y_n\right)=\frac{P\left(Y_1,Y_2,\ldots,Y_n/X\right).P\left(X\right)}{P\left(Y_1,Y_2,\ldots,Y_n\right)} \qquad (16)$$

To simplify the mathematical analysis and computations, we assume that the measurements from different sensors are conditionally independent. Thus, we seek to maximize the likelihood function:

$$h\left(X/Y_1,Y_2,\ldots,Y_n\right)=P\left(Y_1/X\right)^{\alpha_1}\ldots P\left(Y_n/X\right)^{\alpha_n}.P\left(X\right) \qquad (17)$$

Where $0 <= \alpha_p <= 1$, and $p=1, 2, \ldots n$ is defined as the reliability factor of source p. The MRF multisource classification algorithm consists of maximizing $h(X/Y_1, Y_2, \ldots, Y_n)$, which is equivalent to minimizing the energy function:

$$U\left(X/Y_1,Y_2,\ldots,Y_n\right)=\sum_{p=1}^{n}\alpha_p U_p\left(y_s/x_s\right)+U_p\left(x_s/x_{NS}\right) \qquad (18)$$

Specification of the sensor class conditional energy function $U_p(y_s / x_s)$ is given by the first term of equation (4) in section 2. However, the prior energy function is given by equation (13). Note that the multisource data set needs to be co-registered.

4. MRF MULTITEMPORAL CLASSIFICATION

The change of class identity over time can be due to an actual change of information class itself or just due to the change of spectral classes within the same information class. Therefore, by permitting these class changes over time, it is not necessary, in the training stage, to consider all given temporal data sets simultaneously and define additional spectral classes for each information class. Instead, training can be performed separately for each temporal data set. This significantly simplifies the training process. The changes of class identities over time may be modeled by class transition probabilities [3], [11], [14]. Temporal contextual information from temporal neighbors is conveyed to the current classification process via class transition probabilities. So, the multitemporal multisource and contextual classification model is presented as follows:

$$U\left(X^t/Y_1,Y_2,\ldots,Y_n,X^{t-1}\right)=\sum_{p=1}^{n}\alpha_p U_p^t\left(y_s/x_s\right)+U_p^t\left(x_s/x_{Ns}\right)+U_p\left(x_s^t/x_{Ns}^{t-1}\right) \qquad (19)$$

Energy function $U_p(x^t_s / x^{t-1}_{Ns})$ is defined as follows for sensor p:

$$U_p\left(x_s^t/x_{Ns}^{t-1}\right)=-\beta_{temp}\sum_{r\in Ns^{t-1}}Pr\left(x_s^t/x_r^{t-1}\right) \qquad (20)$$

Where $Pr(x^t_s / x^{t-1}_{Ns})$ is the transition probability for a change from class x^{t-1}_{Ns} to class x^t_s between time t-1 and t. βtemp is user specified parameter. Thus, the multitemporal multisource and contextual classification is based on minimizing:

$$U\left(X^t/Y_1,Y_2,\ldots,Y_n,X^{t-1}\right)=\sum_{p=1}^{n}\alpha_p U_p^t\left(y_s/x_s\right)+\beta_{spa}\sum_{r\in q\in Q}I\left(x_s,x_r\right)-\beta_{temp}\sum_{r\in Ns^{t-1}}Pr\left(x_s^t/x_r^{t-1}\right) \qquad (21)$$

5. EXPERIMENTAL RESULTS AND DISCUSSION

The described MRF contextual fusion and classification model is applied to classify a region of interest. Multispectral, multisource and multitemporal images are available upon the north-eastern part of Algiers (Algeria). They are two images of 256X256 pixels. The first one is acquired on June 1997 by HRV-1 sensor of Spot-1 satellite. The second one is acquired on June 2001 by ETM+ sensor of Landsat-7 satellite. To be used in the proposed MRF process, these two images require a pretreatment step (radiometric and geometric corrections). The geographic location of the study area is given on Figure 1. The RGB compositions of the two pretreated images are given on Figure 2 and Figure 3. Four thematic classes dominate the study site: Dense Urban (DU), Bare Soil (BS), Less Dense Urban (LDU) and Vegetation (V). Using a 2-D scatterogram of ENVI software, data samples are selected automatically from each image and from each class for training and testing the proposed classifiers. Statistical assessment of obtained results relatively to the considered test data is performed by using a confusion matrix and two statistical parameters: overall accuracy (OA) and "Kappa" parameter which is computed as follows [4]:

$$Kappa=\frac{N\sum_{i=1}^{M}X_{ii}-\sum_{i=1}^{M}\left(X_{i+}\times X_{j+}\right)}{N^2-\sum_{i=1}^{M}\left(X_{i+}\times X_{j+}\right)} \qquad (22)$$

Where X_{ij} are the confusion matrix elements, X_{i+} is the total sum of elements in lines, X_{j+} is the total sum of elements in columns, X_{ii} are the diagonal elements, *N* is the total number of pixels of the matrix and *M* is the number of considered classes. On the other figures are presented respectively single source and multisource non contextual and contextual classification results, followed by contextual multitemporal results.

Fig 1: Geographic location of the study area (Eastern part of Algiers, Algeria)

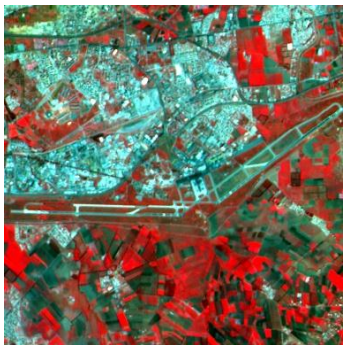

Fig 2: RGB composition of HRV image (1997)

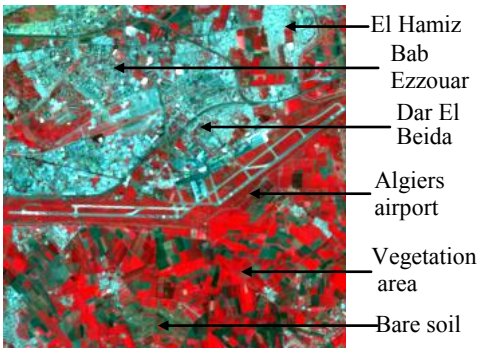

Fig 3: RGB composition of ETM+ image (2001)

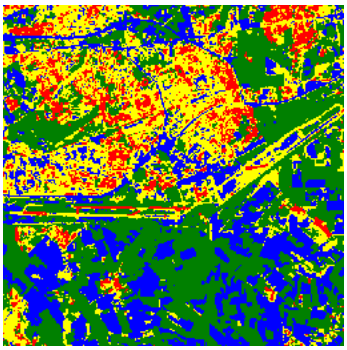

Fig 4: Non contextual classification of HRV image (β_{spa}=0)

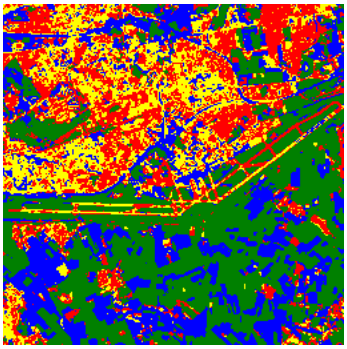

Fig 5: Non contextual classification of ETM+ image (β_{spa}=0)

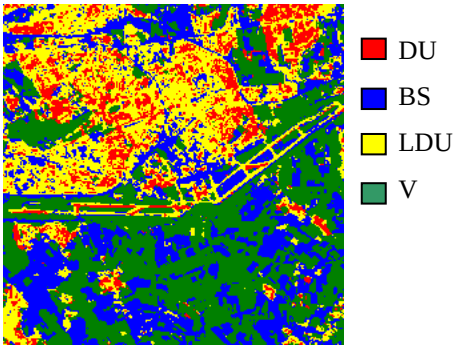

Fig 6: Non contextual multisource fusion and classification (HRV and ETM+) (β_{spa}=0)

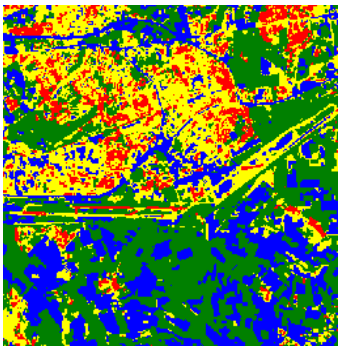

Fig 7: Contextual classification of HRV image (β_{spa}=0.02)

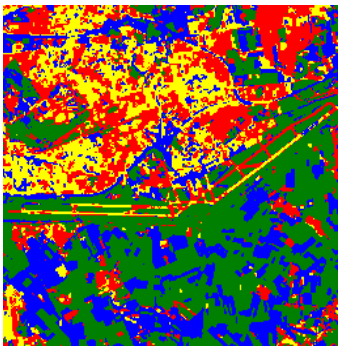

Fig 8: Contextual classification of ETM+ image (β_{spa}=0.08)

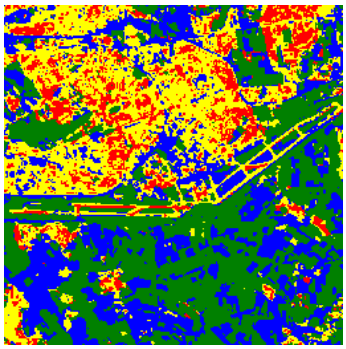

Fig 9: Contextual multisource fusion and classification (HRV and ETM+) (β_{spa}=0.06)

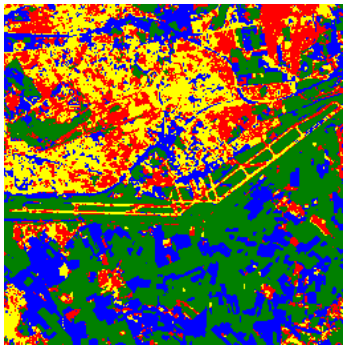

Fig 10: Contextual multitemporal classification (β_{temp}=0.02)

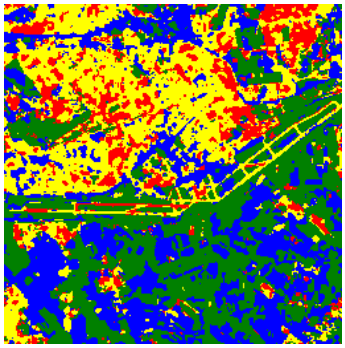

Fig 11: Contextual multitemporal classification (β_{temp}=0.9)

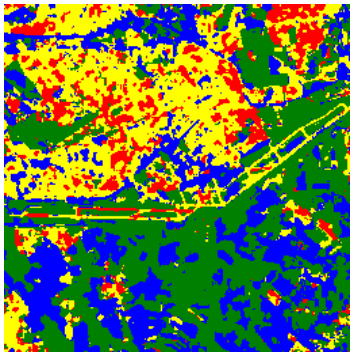

Fig 12: Contextual multitemporal classification (β_{temp}=1)

Statistical assessment of the above obtained results is given on the following Table 1. Notice that the multisource and multitemporal results are evaluated according to a control data base that contains only invariant sites between the two considered dates (1997 and 2001).

Table 1. Statistical assessment of obtained results

Classification result	OA (%)	Kappa
Non contextual HRV (β_{spa}=0)	79.51	0.77
Contextual HRV (β_{spa}=0)	84.27	0.80
Non contextual ETM+ (β_{spa}=0.02)	75.32	0.70
Contextual ETM+ (β_{spa}=0.08)	80.10	0.76
Non contextual multisource (β_{spa}=0)	88.50	0.85
Contextual multisource (β_{spa}=0.06)	92.13	0.89
Contextual multitemporal (β_{temp}=0.02)	81.12	0.78
Contextual multitemporal (β_{temp}=0.9)	78.23	0.75
Contextual multitemporal (β_{temp}=1)	70.04	0.68

Markovian contextual process seems to "clean up" significantly the non contextual (or punctual) classification results. It can be seen that many small isolated pixels are eliminated or reclassified on a correct class, and that each area is much more homogenous. Also, boundaries remain correctly placed. This correct assignment means that each pixel on HRV or ETM+ image, considered in its neighborhood is assigned more accurately. Overall accuracy classification is passed from 79.51% to 84.27% for HRV image, and from 75.32% to 80.10% for ETM+ image. To apply the developed MRF multisource classifier, the reliability factors are statistically estimated as the overall classification accuracy (OA) of each sensor. These factors α_{HRV}=0.69 and α_{ETM}=0.62 are evaluated according to a control data base of invariant sites. For this classifier, only invariant sites (roads, airport lands, etc.) are analyzed because the two images are not acquired on the same time. The BS class is discriminated better by the ETM+ sensor, whereas the LDU class is discriminated better by the HRV sensor. The fusion of the spectral information brought by the high spectral resolution of the ETM+ sensor, and the spatial information brought by the high spatial resolution of the HRV sensor, improve considerably the precision of the classes, in particular the BS and LDU classes. The classification accuracy is better by the integration of the spatial context. The changes occurred during the period between 1997 and 2001 are modeled through the matrix of global changes that we established and that is represented by the following table:

Table 2. Global changes matrix (1997, 2001)

		Reference Image (Classification ICM-HRV)			
		DU	**BS**	**LDU**	**V**
Recent Image (classification ICM-ETM+)	**DU**	**0.25**	0.09	0.39	0.27
	BS	0.03	**0.46**	0.17	0.34
	LDU	0.16	0.17	**0.53**	0.14
	V	0.01	0.25	0.12	**0.62**

This matrix is not diagonal what indicates an important dynamic of the landscape between the two considered dates. The class that underwent the more of changes is the LDU with a rate of 39% toward the DU class. On the other hand, the V class knew fewer changes with a rate of stability of 62%. This global variation is in concordance with the real changes occurred in this region. The MRF multitemporel classifier that we developed requires the specification of the local change matrix mainly to the level of each pixel took in its spatio-temporal context. The weight assigned to this probability of transition is pondered by the parameter β_{temp}. To show the interest of this model, we only considered the multitemporal energy. We have therefore, adopted the spatio-temporal neighborhood 08-connexity (to have a better evaluation of the matrix of local changes) and made vary the parameter β_{temp}. For each value of β_{temp}, a thematic map is generated and evaluated statistically according respectively to the ETM+ control data base, the HRV control data base, and the invariant sites data base. The curves of the following figure illustrate the evolution of the OA parameter according to each data base.

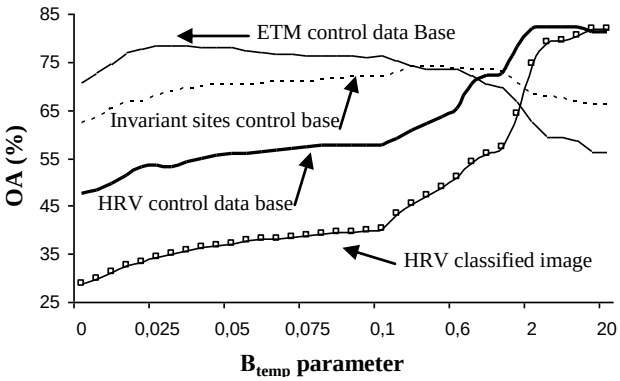

Fig 13: Evolution of classification accuracy according to B

The obtained curves can be distinguished by three types of variations:

1). For $0 < B_{temp} < 0.025$, the evolution is increasing linearly and becomes monotone for all curves. It means that the changes occurred between 1997 and 2001 are not significant. Therefore, the temporal energy plays a role of a regularization term of the recent classification. Thus, the spatio-temporal context of the HRV image contributed considerably for the improvement of the classification of the ETM+ image (see Fig. 10).

2). For $0.03 < B_{temp} < 0.9$, the evolution is increasing linearly for three curves only. The curve drawn relatively to ETM+ control data base is weakly decreasing. This evolution means that the changes occurred between 1997 and 2001 begin to be meaningful. In this case, the transition probabilities pondered by the parameter B_{temp} and added to the data attachment term, encourage the classes of change, what entails the deterioration of the precision of the recent ETM+ classification image. This deterioration touched the DU class that passes to the LDU class mainly, confirming the gradual evolution toward the old classification of 1997 (see Fig. 11).

2). For $B_{temp} > 1$, the evolution is the same that the previous but with a more elevated speed. It means that all pixels of the classified ETM+ image change their original classes toward the classes of HRV image, including the class V that begins to pass in transit to other classes. The multitemporal classification for $B_{temp} = 1$ is given by Fig. 12. The rate of likelihood of this map with the classified HRV image is of 64.11%, and reaches 81.91% for $B_{temp} = 20$.

Thus, while making vary the parameter B_{temp}, we can adjust the weight to assign to the changes occurred between two

different acquirement dates. A more deepened analysis of the obtained results and the realization of other tests by using other types of images, will allow us to establish a relation between the value of the parameter B_{temp} and an included acquirement date between the two initial dates (for our case, between 1997 and 2001). Of this fact, it is possible to generate maps of land cover at any date included between the two initial dates.

6. CONCLUSION

The purpose of this work is to present a robust model for remotely sensed fusion and classification images. Our experience confirms that context information (spectral, spatial and temporal) plays an important role in the task of scene interpretation. At the pixel level, context information provides neighborhood (spectral, spatial, spatio-temporal) information around a pixel, and helps to increase the reliability of each detected object. Discrete random fields, especially the Gibbs Random Fields (GRF) and Markov Random Fields (MRF) provide a methodological framework which allows the integration of context information in satellite data fusion and classification. A power of these models is that the prior probability density function modeled by the use of the contextual information and the class conditional probability density function modeled by the use of the observed data from one or more sensors, can be easily combined through the use of suitable energy function. Once the posterior energy model and the associated parameters have been defined, pixel labeling is found out by using the MAP estimate which is equivalent to a minimum energy function in terms of GRF-MRF modeling. For a non-convex energy function, the solution space may contain several local minims. To find a global minimum which is a truly MAP estimate, the solution is to use an optimization algorithm among which ICM is the most know and used. The ICM algorithm is sub-optimal and converges only to a local minimum of the energy function. However, classification result of such algorithm is acceptable and shows that the incorporation of contextual information successfully improves classifier performances by more than 10% in terms of global accuracy. Also, by including the temporal context of data, the model is suitable for detecting class changes over time. However, algorithms and methods to construct more complex models and to efficiently integrate context (spectral, spatial, and temporal) in order to achieve higher classification accuracy, are still significant issues worthy of further investigation.

7. REFERENCES

[1] Besag, J. 1986. On the Statistical Analysis of Dirty Pictures. *Journal Royal of Statistics: Soc. B, 48, 3, pp. 259-302.*

[2] Braathen, B., Pieczynski, W., and Masson, P. 1993. Global and local methods of unsupervised Bayesian segmentation of images. *Machine Graphics and vision, vol. 2, no. 1, pp. 39-52.*

[3] Byeungwoo, J., and Landgrebe, D. A. 1999. Decision Fusion Approach for Multitemporel Classification. *IEEE Transactions on Geoscience and Remote Sensing, vol. 37, no. 3, pp.1227-1233.*

[4] Congalton, R. G., 1991. A Review of Assessing the Accuracy of Classifications of Remotely Sensed Data. *Remote Sensing of Environment, no. 37, pp. 35-46.*

[5] Descombes, X., Morris, R. D., Zerubia, J., and Berthod, M. 1999. Estimation of Markov Random Field Prior Parameters Using Markov Chain Monte Carlo Maximum Likelihood. *IEEE Trans. Geosci. Remote Sensing, vol. 8, no. 7, pp. 954-962.*

[6] Geman, S., and Geman, D. 1984. Stochastic Relaxation, Gibbs Distribution, and the Bayesian Restoration of Images. *IEEE Trans. Pattern Analysis and Machine Intelligence, PAMI-6, pp. 721-741.*

[7] Kheddam, R., and Belhadj-Aissa, A. 2001. General Multisource Contextual Classification Model of Remotely Sensed Imagery based on MRF. *IEEE / ISPRS Workshop on Remote Sensing and Data Fusion Over Urban Areas, Rome, Italy.*

[8] Kheddam, R., Belhadj-Aissa, A., and Ranchin, T. 2002. Study of ICM parameters influence on imges satellite contextual classification. *In proceedings of the 22nd symposium of the European association of remote sensing laboratories, Prague, Czech, pp. 79-85.*

[9] Marroquin, J., Mitter, S., Poggio, T. 1987. Probabilistic solution of ill-posed problems in computational vision. *Journal of the American Statistical Association, no. 82, pp. 76-89.*

[10] Pieczynski, W. 1989. Estimation of context in random fields. *Journal of Applied Statistics, vol. 16, no. 2, pp. 283-289, 1989.*

[11] Schistad Solberg, A. H., Taxt, T., and Jain, A. K. 1993. Fusion of multitemporal satellite images and GIS data for land-use classification. *In Proc. 8th Scandinavian Conf. Image Analysis, Tromso, Norway, Technical report.*

[12] Schistad Solberg, A. H., Taxt, T., and Jain, A. K. 1994. Multisourse classification of remotely sensed data: Fusion of Landsat TM and SAR images. *IEEE Transactions on Geosciences and Remote Sensing, vol. 32, pp. 768-778.*

[13] Schistad Solberg, A. H., Taxt, T., and Jain, A. K. 1996. A Markov random field model for classification of multisource satellite imagery. *IEEE Transactions on Geosciences and Remote Sensing, vol. 34, no. 1, pp. 100-113.*

[14] Schistad Solberg, A. H. 1999. Contextual data fusion applied to forest map revision. *IEEE Transactions on Geosciences and Remote Sensing, vol. 37, no. 3, pp. 1234-1243.*

[15] Wald, L. 1999. Some terms of reference in data fusion. *IEEE Transactions on Geosciences and Remote Sensing, 37, 3, pp.1190-1193.*